Biomaterials 91 (2016) 11–22

Contents lists available at ScienceDirect

Biomaterials

journal homepage: www.elsevier.com/locate/biomaterials

Engineering EMT using 3D micro-scaffold to promote hepatic functions for drug hepatotoxicity evaluation

Jingyu Wang [a], Fengling Chen [b], Longwei Liu [c], Chunxiao Qi [a], Bingjie Wang [c], Xiaojun Yan [a], Chenyu Huang [d], Wei Hou [e], Michael Q. Zhang [b], Yang Chen [b, **], Yanan Du [a, f, *]

[a] Department of Biomedical Engineering, School of Medicine, Collaborative Innovation Center for Diagnosis and Treatment of Infectious Diseases, Tsinghua University, Beijing, 100084, PR China
[b] MOE Key Laboratory of Bioinformatics, Bioinformatics Division & Center for Synthetic and Systems Biology, Department of Automation, TNLIST, Tsinghua University, Beijing, 100084, PR China
[c] The School of Life Science, Tsinghua University, Beijing, 100084, PR China
[d] Department of Plastic, Reconstructive and Aesthetic Surgery, Beijing Tsinghua Changgung Hospital, Medical Center, Tsinghua University, Beijing, 102218, PR China
[e] Tianjin Second People's Hospital and Tianjin Institute of Hepatology, Tianjin, 300192, PR China
[f] China Orthopedic Regenerative Medicine Group (CORMed), Hangzhou, Zhejiang, 310058, PR China

ARTICLE INFO

Article history:
Received 21 February 2016
Accepted 1 March 2016
Available online 9 March 2016

Keywords:
EMT
3D micro-scaffold
Hepatic functions
HDACs
Drug hepatotoxicity evaluation

ABSTRACT

Accompanied by decreased hepatic functions, epithelial-mesenchymal transition (EMT) was observed in two dimensional (2D) cultured hepatocytes with elongated morphology, loss of polarity and weakened cell-cell interaction, while upgrading to 3D culture has been considered as significant improvement of its 2D counterpart for hepatocyte maintenance. Here we hypothesize that 3D culture enhances hepatic functions through regulating the EMT status. Biomaterial-engineered EMT was achieved by culturing HepaRG as 3D spheroids (SP-3D) or 3D stretched cells (ST-3D) in non-adherent and adherent micro-scaffold respectively. In SP-3D, constrained EMT of HepaRG, a hepatic stem cell line, as represented by increased epithelial markers and decreased mesenchymal markers, was echoed by improved hepatic functions. To investigate the relationship between EMT status and hepatic functions, time-series RNA-Seq and gene network analysis were used for comparing different cell culture models, which identified *histone deacetylases* (*HDACs*) as key mediating factors. Protein analysis confirmed that high HDAC activity was correlated with high expression of *Cadherin-1* (*CDH1*) and hepatic function genes, which were decreased upon HDAC inhibitor treatment in SP-3D, suggesting *HDACs* may play positive role in regulating EMT and hepatic functions. To illustrate the application of 3D micro-scaffold culture in drug safety evaluation, hepatotoxicity and metabolism assays of two hepatotoxins (*i.e.* N-acetyl-*p*-aminophenol and Doxorubicin) were performed and SP-3D showed more biomimetic toxicity response, indicating regulation of EMT as a vital consideration in designing 3D hepatocyte culture configuration.

1. Introduction

Drug induced hepatotoxicity is one of the major causes for drug withdrawal from market, which is a huge loss for both patients and pharmaceutical companies [1]. Primary hepatocytes, the gold standard in drug hepatotoxicity screening, quickly lose hepatic functions *in vitro* [2]. Alternatives, such as hepatoma cell lines or stem cell derived hepatic-like cells, on the other hand, face problems of early de-differentiation in culture leading to lack of relevant gene expressions, loss of epithelial polarity, specific protein synthesis and critical enzyme activity [3–5]. Recently, researches revealed that culturing in 3D *in vitro* configurations, such as in bioreactors or hydrogels, could offer biomimetic micro-environments to maintain hepatic functions of hepatocytes and promote hepatic differentiation of stem cells for drug screening and

* Corresponding author. Department of Biomedical Engineering, School of Medicine, Collaborative Innovation Center for Diagnosis and Treatment of Infectious Diseases, Tsinghua University, Beijing, 100084, PR China.
** Corresponding author.
E-mail addresses: yc@tsinghua.edu.cn (Y. Chen), duyanan@tsinghua.edu.cn (Y. Du).

http://dx.doi.org/10.1016/j.biomaterials.2016.03.001
0142-9612/

potential clinical treatments [6–9]. However, molecular mechanism as to how 3D culture, when compared to 2D culture, improves hepatic functions is not well understood.

In 2D culture, the morphological change of hepatocytes was observed from polygonal to elongated, accompanied by decreased hepatic functions [10]. Such morphological change also occurs during typical epithelial-mesenchymal transition (EMT) in cell culture [11]. EMT, and its transverse process, mesenchymal-epithelial transition (MET) are mainly observed in embryo development, tissue fibrosis, and tumor metastasis [12,13]. EMT/MET are continuous processes which are characterized by expression of representative epithelial markers [*e.g.* E-cadherin (E-cad)] and mesenchymal markers (*e.g.* Vimentin) respectively. Both bioactive factors (*e.g.* TGFβ) and biophysical approaches have been shown to regulate the process of EMT/MET [14–17]. As examples of biophysical regulation of EMT, microgrooves fabricated on 2D surface enhanced MET in fibroblasts to improve the efficiency of their de-differentiation into induced pluripotent stem cell (iPSC) [16,18]. Also, substrate stiffness-induced translocation of an EMT-related protein, TWIST, from cytoplasm to nuclear was found to promote EMT and invasion of breast cancer cells [19].

Here we hypothesize that improved hepatic functions in 3D culture configurations as compared to 2D culture are realized by regulating the EMT status of hepatic cells. In our previous study, cells cultured in gelatin (adherent) and PEGDA (non-adherent) micro-scaffold showed representative features of mesenchymal and epithelial status with stretched 3D (ST-3D) and spheroid 3D (SP-3D) morphology respectively [20–22]. In this work, systemic characterization of hepatic functions and EMT status in ST-3D, SP-3D and traditional 2D culture configurations confirmed the correlation between the enhanced MET and the improved hepatic functions at both gene and protein level. Through transcriptome analysis of cells cultured in these three configurations, histone deacetylases (HDACs) were revealed to be the most critical regulatory factors between EMT and hepatic functions. Acetylation, regulated by HDACs and histone acetyltransferase (HAT), is among the best understood post-translational modifications of histones and increased acetylation level is associated with increased transcription level of specific genes [23]. Different types of inhibitors, *e.g.* Trichostatin A (TSA), have hence been developed to regulate HDACs for induction of specific changes in genes expression involved in a variety of cellular processes (*e.g.* apoptosis) [24]. HDACs activities were also shown to be modulated by biophysical cues [25]. For example, localization of HDAC3 could be re-arranged to switch gene expression patterns by altering cell-substrate interactions and cellular geometry [26].

This study aims to provide insight into the mechanism of how hepatic functions are promoted in 3D culture, thus establishing design criteria for engineering system for hepatocyte-based basic research and applications. Hepatocytes maintained in *in vitro* models are expected to possess major metabolic enzymes in functional liver to recapitulate drug metabolism *in vivo*. The metabolic enzymes are typically divided into Phase I: those that induce basic alteration of structures [*i.e.* Cytochrome 450s (CYP 450)] and Phase II: those that induce conjugation of a hydrophilic moiety (*e.g.* uridine diphosphate glucuronosyltransferase (UGT) 1A1) [27,28]. We used HepaRG, a hepatic stem cell line, which can further differentiate into hepatocyte and cholangiocyte *in vitro,* and is hence highly valued for application in drug hepatotoxicity evaluation and metabolism analysis [29,30]. Phase I and phase II drug metabolic enzymes in HepaRG were confirmed to be present in 2D monolayer culture and various 3D culture configurations [31,32]. To demonstrate its application in drug safety evaluation, HepaRG cultured in 2D, ST-3D and SP-3D were treated with two clinically-proven hepatotoxins (*i.e.* N-acetyl-*p*-aminophenol and Doxorubicin) with different metabolic pathways in hepatic cells. Based on their respective half maximal inhibitory concentration (IC50) in the three culture configurations, it is evident that better biomimicry of physiological drug response was recapitulated in SP-3D culture as compared in ST-3D or 2D culture. This further asserts on the importance of EMT as a vital criterion for consideration during biomaterial designs for hepatocyte-based application.

2. Materials and methods

1. Materials

All the reagents were purchased from Alladdin (China) unless otherwise indicated.

2. HepaRG culture

HepaRG cells were maintained in William's E medium (Gibco, USA) supplemented with 10% fetal bovine serum (FBS, Wisent, Canada), 50 units/mL penicillin and streptomycin (Wisent, Canada), 2 mM GlutaMax (Gibco, USA), 5 μg/mL insulin, and 0.5 μM hydrocortisone hemisuccinate, as previously described [33]. To visualize the efficiency of hepatic differentiation, plasmid containing human albumin (ALB) promoter and enhanced green fluorescent protein (EGFP) (ALB promoter-EGFP) sequence was constructed and transduced into HepaRG using lentivirus (packaged in HEK293T cells and concentrated by ultracentrifugation) [34]. ALB promoter-EGFP transduced HepaRG was only used for imaging in 3D micro-scaffold while the wild type HepaRG were used for the rest experiments.

3. Autoloading of HepaRG into micro-scaffold

Gelatin and poly (ethylene glycol) diacrylate (PEGDA) micro-scaffolds were prepared as described before and exposed under UV for sterilization before cell seeding (Please see Supplementary methods for details) [21,35]. 60 μl single cell suspension (5×10^6 cells/mL) was pipetted onto the micro-scaffold monolayer in 35 mm dish and automatically absorbed to hydrate the porous scaffold. The dish was maintained in a humidified chamber and incubated at 37 °C for 30 min to allow for cell attachment. Then the micro-scaffold monolayer was transferred by tweezers to 24-well plate with 1 mL medium for further culture and experiments.

4. Cell viability analysis

To evaluate cell viability and number, CellTiter Blue (Promega, USA) assay was performed according to manufacturer's instruction. Briefly, after PBS washing, 300 μL mixture of CellTiter Blue and medium (1:5) was added to the wells. After incubation at 37 °C for 2 h, signal was detected with a microplate reader (560 nm/590 nm, SpectraMax M5, Molecular Devices, USA).

5. Staining and imaging

For F-actin staining, Rhodamine/phalloidin (Cytoskeleton, USA) and Hoechst 33342 (Sigma-Aldrich, USA) were used according to manufacturer's instruction and a Zeiss confocal microscope (LSM710, Germany) was used for imaging. For immunohistochemical and HE staining, paraffin-embedded tissue sections (5 μm) were deparaffinized and rehydrated in graduated alcohol. After antigen retrieval using sodium citrate buffer, sections were incubated in anti-occludin antibodies (diluted as 1:50, Santa Cruz Biotechnology, USA) overnight at 4 °C. Stained tissue sections were visualized using secondary antibody and 3, 3-diaminobenzidin

(DAB, ZSGB-Bio, China) under microscope. Hematoxylin-eosin (HE) staining was performed based on standard protocols [36].

6. Real time reverse transcription-polymerase chain reaction (RT-PCR)

Gene expression was examined by RT-PCR analysis using protocols previously described [37]. Total RNA was extracted by TRIZOL reagent and reversely transcribed using first-strand cDNA synthesis kit (Takara, China) according to the manufacture's protocol. Real-time RT-PCR was performed using SYBR Green II (Takara, China) and inventoried assay on Bio-Rad CFX96 Real-Time PCR platform (USA). The housekeeping gene, *glyceraldehyde 3-phophate dehydrogenase (GAPDH)*, was used as an internal control for normalization. Gene specific primers were synthesized by Sangon Biotech (China) and their sequences were listed in Table S5.

7. Immunoblotting

Western blotting was carried out as previously described [37]. Briefly, total protein from HepaRG in micro-scaffold or 2D was extracted using RIPA lysis buffer (Beyotime, China) supplemented with 100× protease inhibitors Phenylmethanesulfonyl fluoride (PMSF, Beyotime). Proteins were separated on polyacrylamide gels, transferred by electroblotting on to PVDF membrane (Millipore, USA) and detected through secondary antibodies and SuperSignal West Pico Chemiluminescent Substrate (Thermo, USA) and imaged by ChemiDoc XRS+ with image Lab software (Bio-Rad, USA). The following dilutions were used for primary antibodies: rabbit anti-ALB (1:500, Dako, Denmark); mouse anti-E-cad (1:500, Abcam, USA); rabbit anti-Vimentin (1:500, Merck Millipore, Germany); rabbit anti-acetyl-Histone H3 (1:500, Abcam, UK); rabbit anti-GAPDH (1:800, Santa Cruz Biotechnology, USA); mouse anti-β-actin (1:1000, CMCTAG, USA). The dilutions for secondary antibodies (ZSGB-Bio, China) were 1:5000.

8. ALB and urea production

After 5 days or 28 days of culture, culture medium was exchanged with fresh medium which was collected 24 h later [38]. Total ALB and urea production were detected by enzyme-linked immunosorbent assay (ELISA) kit (Bethel laboratories, USA) and QuantiChrom Urea Assay Kit (BioAssay Systems, USA) respectively according to the manufacturer's recommendations. Protein production was normalized to cell number determined by CellTiter Blue as described before. HepaRG culture medium was used as blank control.

9. RNA-Seq and analysis

Total RNA of HepaRG in 2D, ST-3D and SP-3D on Day 1, 3 and 5 was extracted using TRIZOL as described before. After library construction and sequencing, gene expression level was quantified in reads per kilobase of exon model per million mapped reads (FPKM) with common workflow using Tophat and Cufflinks [39]. Correlation coefficient between gene expression level of each two samples was calculated and drawn as the correlation heatmap. Hierarchical clustering was performed in both gene and sample dimension and drawn as bi-clustering heatmap. To identify critical linkage between EMT/MET and differentiation, calculation and screening were performed at three levels. Firstly, differentially express genes (DEGs, Table S1) of expression changes >2 or <0.5 were identified using classic edgeR analysis between each pair of culture conditions [40]. In comparison, samples at three time points of one culture condition were treated as triplicates based on similar gene expression pattern shown by heatmap to identify DEGs. DEGs between different culture conditions were used for biological process enrichment with DAVID, an online functional annotation analyzer and further analysis [41]. Secondly, the shortest paths between EMT marker *CDH1* and the hepatic function related genes (Table S3) were identified using R package iGraph in background network, which was merged by protein-protein interaction (PPI) network from the Human Protein Reference database [42] and gene regulatory network from HTRI database [43,44]. Among multiple shortest paths between *CDH1* and each hepatic function related gene, those with most DEGs were selected as the most probable paths. All probable paths between *CDH1* and every hepatic function gene listed in Table S3 constituted networks were shown in Fig. 4 and Fig. S11. Thirdly, linkage betweenness score of all genes in four networks were calculated with Q-measure and ranked to evaluate the importance of each gene in connecting *CDH1* and hepatic function related genes (Table S4) [45]. The gene with highest linkage betweenness score in each work was selected as most critical linkage between EMT and hepatic functions.

10. HDACs inhibition

HDAC inhibitor Trichostatin A (TSA, Stelleck, USA) was applied as noncompetitive inhibitor by mimicking the lysine substrate of histone, which reduced binding between HDACs and histone [46]. TSA was dissolved in DMSO (Biomol, USA) at 20 mM for long term storage at −20 °C. Aliquots of stock solutions of 100 μM were prepared and stored in −20 °C. Based on optimization with TSA concentration gradient from 125 nM to 2 μM, the final concentration of TSA used in HepaRG culture was 250 nM, in which the final DMSO concentration was 0.25%. After 2 days' culture in 2D, ST-3D and SP-3D, HepaRG were treated with either TSA (250 nM) or vehicle (0.25% DMSO) for another 3 days. Then RNAs or proteins were extracted as described above for further analysis.

11. APAP and Dox hepatotoxicity evaluation

HepaRG cultured for 5 days were treated with desired concentrations of N-acetyl-*p*-aminophenol (APAP, J&K, China) or Doxorubicin hydrochloride (Dox). Both drugs were kept in DMSO under −20 °C and diluted with fresh medium directly before use. After 24 h administration, cell viability was determined by CellTiter Blue assay and response curves were plotted as normalized cell viability rates against drug concentrations to calculate the half maximal inhibitory concentration (IC50).

To detect APAP metabolite, 10 μM Dexamethasone (Dex, Sigma-Aldrich, USA) was added to induce the activity of CYP3A enzymes of HepaRG 48 h prior to APAP treatment. After 24 h APAP administration, HepaRG in culture was washed with PBS and extracted using 95% methanol followed with 30 min ultrasound treatment. The supernatant after centrifugation for 5 min at 10000 g was collected, lyophilized and re-suspended in methanol for APAP metabolite detection using LC-MS/MS (Q-Exactive, Thermofisher Scientific, USA) [47] [48]. Please see Supplementary method for details.

To detect Dox retention, HepaRG were treated with Dox (5.75 μM) with or without Celecoxib, a MDR1 inhibitor (25 μM). 24 h later, HepaRG cells were trypsinized to single cells and their fluorescence intensities of 488−580 were detected by flow cytometry. Cells without Dox treatment in 2D culture were set as negative control.

12. Statistical analysis

Statistical analysis was performed by GraphPad Prism. Significance of differences between groups was checked using students *t*-

test. All data were presented as mean values ± standard deviation (SD). Three independent experiments per assay were carried out unless otherwise indicated.

3. Results

3.1. ST-3D and SP-3D culture of HepaRG in micro-scaffold based 3D culture configuration

Two types of micro-scaffold based on gelatin and PEGDA, were fabricated using established methods in our previous work [21,22,49] and shown in Fig. 1A. SEM images revealed that HepaRG were stretched with elongated morphology when attached to the bio-adhesive gelatin scaffolds (ST-3D), while formed tiny spheroids in non-adherent PEGDA scaffolds (SP-3D) (Fig. 1B). The spheroid diameters in SP-3D mostly fell in the range of 50–80 μm, regardless of the initial seeding density (Fig. S1). The uniform spheroid formation may be due to the relative uniformity of pore sizes of PEGDA scaffolds (See Supplementary method). Microvilli structure was also observed in SP-3D culture as shown by SEM (Fig. 1B) and TEM (Fig. S2). In particular, TEM images showed that polarized distribution of Golgi complex was found at cytoplasmic regions of HepaRG, especially regions adjacent to the neighboring cells, but not adjacent to the scaffold. 3D reconstructed fluorescence images, revealed uniform distribution of ALB promoter-EGFP transduced HepaRG in gelatin or PEGDA micro-scaffold after 5 days (Fig. 1C, D). In addition, brighter EGFP expression of HepaRG in PEGDA micro-scaffold than those in gelatin micro-scaffold further suggested that SP-3D culture configuration promoted hepatic functions (*i.e.* ALB expression) of HepaRG. HE staining indicated that there was no necrosis core formation during spheroid culture (Fig. 1E) and Occludin, a protein involved in tight junction formation between adjacent hepatocytes, was observed, indicating strong cell-cell interaction in SP-3D but not in ST-3D (Fig. 1F). F-actin expression was mainly distributed between adjacent cells in SP-3D, suggesting strong cell-cell interactions, while cells distributed along the scaffold fibers in ST-3D presented intense cytoskeleton throughout the entire cell body (Fig. 1G).

3.2. Improved hepatic functions in SP-3D over ST-3D

To characterize hepatic functions of spontaneously differentiated HepaRG in 3D culture, related hepatic function protein and gene expressions were analyzed. In comparison with ST-3D, drastic increase in ALB expression was observed in SP-3D at both gene and protein level (Fig. 1H, I). Expression of critical hepatic transcription factors, *hepatocyte nuclear factor 4 alpha (HNF4α)* and *tyrosine aminotransferase (TAT)*, in SP-3D showed 4-fold and 2.5-fold increase respectively when compared with ST-3D. *Peroxisome proliferator-activated receptor (PPARα)*, involved in lipid homeostasis in liver, showed a 15-fold increase in SP-3D. *Pregnane X receptor (PXR)*, a xenobiotic sensor during drug metabolism, was expressed higher in SP-3D than ST-3D (Fig. 1I). Three isoforms of cytochrome P450 enzymes (CYP 450s), *1A2, 3A4, 3A7*, as Phase I metabolic enzymes, showed about 5-fold higher expression in SP-3D than in ST-3D (Fig. 1J). Expression of *glutathione S-transferase A1 (GSTA1)*, *uridine diphosphate glucuronosyltransferase (UGT) 1A1* and *1A2*, as Phase II metabolic enzymes, were elevated 20-fold, 2-fold and 3-fold in SP-3D respectively (Fig. 1K). Genes of *ATP-Binding Cassette, Sub-Family B, Member 1* [*ABCB1*, also known as *multidrug resistance protein 1 (MDR1)*], *ATP-Binding cassette, sub-family C, member 2* [*ABCC2*, also known as *multidrug resistance-associated protein 2 (MRP2)*] and another two homologs, *ABCC3* (*MRP3*) and *ABCC6 (MRP6)*, were found to be highly expressed in SP-3D, but not in ST-3D. *ABCB1*, one of the most important transporters for drug resistance, was down-regulated in SP-3D, which was consistent with decreased expression during liver maturation *in vivo* (Fig. 1L) [50]. Meanwhile, higher protein expression of E-cad [coded by *Cadherin-1* (*CDH1*)], while lower protein expression of Vimentin, a mesenchymal marker, was observed in SP-3D than in ST-3D, which suggested different EMT status of HepaRG in these two culture configurations (Fig. S3, Fig. S4).

3.3. Concordance of MET with improved hepatic functions

To systematically study the relationship of EMT status and hepatic functions in *in vitro* HepaRG culture, traditional 2D culture was introduced as control as it is well known to result in EMT and poor hepatic functions [51,52]. In three culture configurations, cell numbers reached saturation at Day 5 (Fig. S6), hence day 5 was chosen to be the end point for following characterization. Hepatic functions of HepaRG were then further characterized in the three culture configurations by normalized ALB and urea production (Fig. 2A–B). Both ALB and urea production level were the lowest in 2D, moderate in ST-3D and highest in SP-3D. Characterization of EMT status was quantified by relative EMT-related gene expression. Generally, expression of epithelial markers, *CDH1* and *epithelial cell adhesion molecule (EpCAM)* increased from 2D, ST-3D to SP-3D, while that of mesenchymal markers, *Snail family zinc finger 1 (Snail)*, *Twist Family BHLH Transcription Factor 1 (Twist)*, *Vimentin* and *Cadherin-2* [*CDH2*, also known as *neural cadherin(N-cad)*] decreased from 2D, ST-3D to SP-3D (Fig. 2C–F) [53]. Notably, with increasing culture time, significant up-regulation in *CDH1* and *EpCAM* expression and likewise, down-regulation in *Snail, Twist, Vimentin* and *N-cad* expression, was occurrence of MET during SP-3D culture. Statistical analysis of comparison between each pair of the 6 EMT genes was listed in Fig. S8.

3.4. Transcriptome analysis revealed HDACs as key regulators between EMT and hepatic functions

To identify potential regulators or mediators between EMT status and hepatic functions, global gene expression of HepaRG in 2D, ST-3D and SP-3D at three time points (Day 1, 3, 5) was analyzed using RNA-seq. General trend of gene expression levels in these three culture configurations was consistent with that obtained from qPCR (Fig. S10-11). Correlation heatmap revealed that 2D culture configuration led to drastically different gene expression pattern from its 3D counterparts, especially from the SP-3D culture (Fig. 3A). The difference in gene expression pattern between 2D and 3D was observed as early as Day 1. For direct comparison of similarity in gene expression patterns between each two specific conditions (*i.e.* culture configuration and duration), bi-clustering analysis was performed, which showed clustering of genes mostly occurred between conditions within the same culture configurations, but not between the same culture durations (Fig. 3B). Therefore, conditions from three culture durations in the same configuration were taken as triplicates to identify differentially expressed genes (DEGs). In total, classic edgeR analysis identified 4427 DEGs between SP-3D and 2D, 3348 DEGs between ST-3D and 2D and 231 DEGs between ST-3D and SP-3D (Fig. 3C, Table S1). Again, it proved that the most significant difference occurred between the 3D configurations and their 2D counterpart. Meanwhile the most significant difference between SP-3D and ST-3D was shown on Day 5 with 988 DEGs. To categorize DEGs, gene ontology (GO) analysis was performed and the most significant GO terms of DEGs [with false discovery rate (FDR) < 0.05] were listed in Table S2. As represented by top 10 GO terms of DEGs (SP-3D VS 2D) in Fig. 3D, up-regulated DEGs were mainly related to metabolic/biosynthetic processes (including lipid, steroid and cholesterol

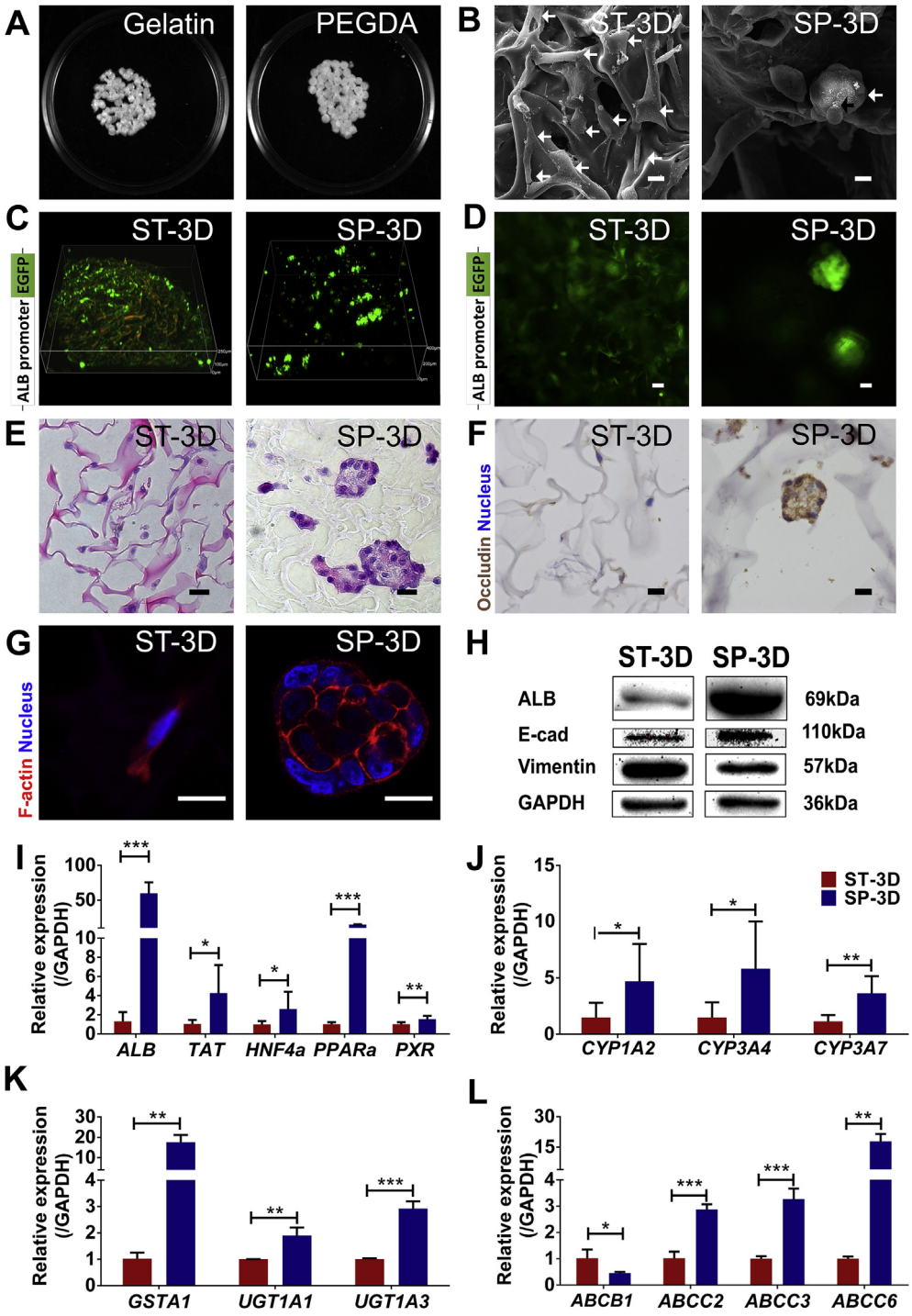

Fig. 1. Improved hepatic functions in SP-3D vs ST-3D. A. Photos of ready-to-use gelatin and PEGDA micro-scaffolds clustered as a monolayer in 35 mm dishes. B. SEM images of HepaRG in 3D culture. White arrow: HepaRG cells. Black arrow: bile canaliculus formed between adjacent cells in spheroid. C. 3D reconstructed fluorescence images of ALB promoter-EGFP transduced HepaRG. D. Fluorescence images of pALB-EGFP transfected HepaRG taken at the same setting in ST-3D and SP-3D. E. HE staining of sectioned HepaRG in 3D culture. F. Occludin staining. G. Confocal images of F-actin staining. Scale bar: 20 μm. H. WB of ALB, E-cad and Vimentin with quantitative statistics in Fig. S2. I–L. RT-PCR analysis of hepatic function gene expression normalized with *GAPDH*. (*: $P < 0.05$, **: $P < 0.01$, ***: $P < 0.001$).

metabolism) and immune/inflammation (commonly involved in regulation of MET), while down-regulated DEGs were mainly related to cell division and cell cycle, which might explain the low cell proliferation rate in SP-3D (Fig. S6) [54].

To establish for linkage between EMT and hepatic functions, identified DEGs were used as reference genes to construct gene networks between EMT marker *CDH1* (gene symbol of E-cad) and hepatic function genes (Table S3). The network constructed between SP-3D and 2D connected *CDH1* with 88 hepatic function genes (covered one third of the function gene list) through mediators including well-known hepatic transcription factors such as *HNF1A* and CEBP families (Fig. 4, Fig. S12A) [44]. To further search for key mediators within the network, linkage betweenness were scored and ranked by network topology analysis with Q-measure

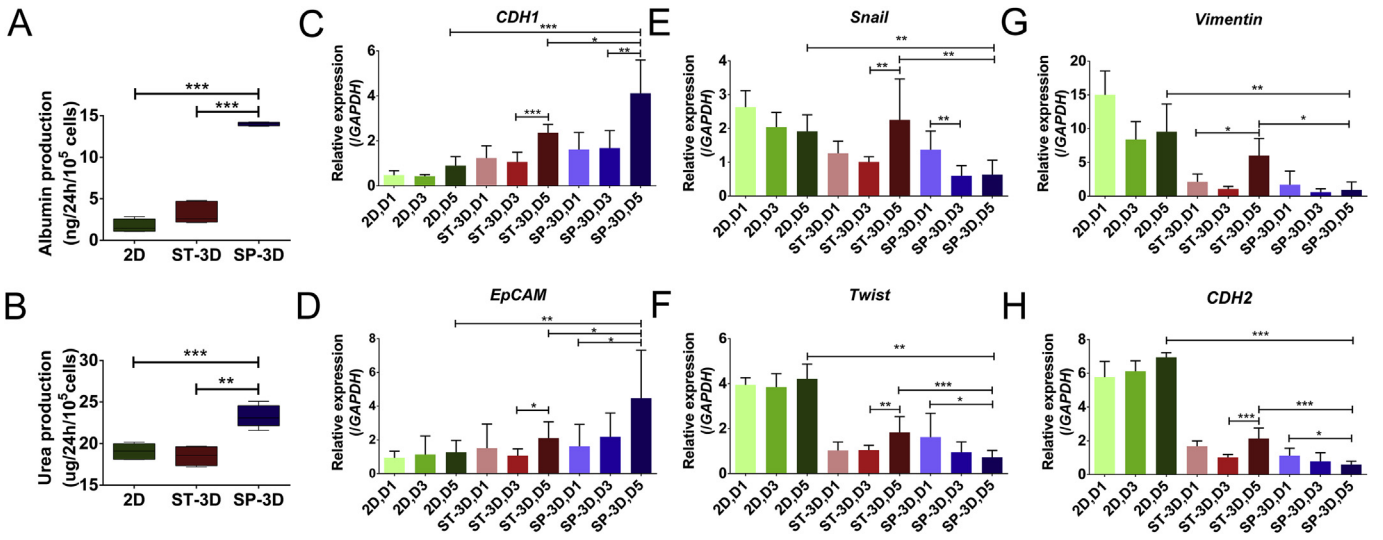

Fig. 2. Concordance of MET with improved hepatic functions. A. Albumin production detected by ELISA. B. Urea production. C–H. RT-PCR analysis of EMT marker expression normalized with *GAPDH*. Detailed statistical analysis of differences between each two conditions was listed in Fig. S8. (*: $P < 0.05$, **: $P < 0.01$, ***: $P < 0.001$).

(Table S4). *Histone deacetylases (HDACs)*, with the highest linkage betweenness score, were identified to be the most important mediator between *CDH1* and hepatic function genes. Similarly, the networks constructed using DEGs obtained from ST-3D vs 2D and SP-3D vs ST-3D also identified *HDACs* as key mediators between *CDH1* and hepatic function genes (Fig. S12 B, C).

3.5. Correlation of HDACs with E-cad and hepatic functions

As deacetylation is the key function of HDACs, western blot of acetylation of histone 3 (AcH3) of HepaRG was performed to characterize the status of histone acetylation in the three culture configurations (Fig. 5A). Acetylation was decreased in accompany with increase in ALB and E-cad expression (Fig. 1), suggesting elevated HDAC activity in SP-3D compared with ST-3D or 2D. Hence, HepaRG in SP-3D were selected to be treated with HDACs inhibitors, aiming to test whether blockage of HDAC activity would induce decreased hepatic functions (Fig. 5B). During optimization of TSA (a general HDACs inhibitor) administration, severe cell death was observed when HepaRG were treated with TSA of more than 500 nM, hence 250 nM TSA was used for blockage of HDAC activity (Fig. S13). After TSA treatment, gene expression of *HDAC1* and *HDAC2* were both slightly down-regulated. Meanwhile, *CDH1* expression was decreased and *CDH2* expression was increased (Fig. 5C). Gene expression levels of *ALB* and *CYP1A2* as representative hepatic functions were also decreased after TSA treatment in SP-3D, which was consistent with our expectation.

3.6. Application of SP-3D and ST-3D in drug toxicity and metabolism evaluation

To demonstrate the application of these versatile 3D micro-scaffold culture configurations in drug hepatic toxicity and metabolism evaluation, APAP and Dox, two prescribed drugs commonly known for their hepatotoxicity were tested in HepaRG cultured in ST-3D and SP-3D (Fig. 6). Significant increase in sensitivity of HepaRG to APAP-induced toxicity was found in SP-3D when compared to ST-3D and 2D (Fig. 6A). The obtained IC50 of APAP was 45.38 mM, 5.869 mM and 2.487 mM in 2D, ST-3D and SP-3D respectively. The difference was due to the improved metabolic functions of HepaRG in SP-3D, as evident from increased production of APAP metabolites [*i.e.* 4-acetamidophenyl-beta-D-glucuronide (APAP-Glc) and acetaminophen glutathione (APAP-Glth)] (Fig. 6B).

In contrast, resistance of HepaRG against Dox was more prominent in SP-3D, with IC50 of 6.746 μM, 18.35 μM and 55.86 μM in 2D, ST-3D and SP-3D respectively (Fig. 6C). Significant differences in IC50 between each groups indicated less sensitivity of HepaRG in SP-3D against Dox than ST-3D or 2D. To verify that Dox efflux was relied on *ABCB1* coded MDR1 (a major efflux transporter of drugs), Celecoxib (a MDR1 inhibitor) was added along with Dox in culture medium. In presence of Celecoxib, Dox retention within HepaRG increased in all the three configurations without changing the trend (SP-3D < ST-3D < 2D), indicating MDR1 activity was responsible for the reduced sensitivity against Dox in SP-3D (Fig. 6D).

4. Discussion

In this study, engineered EMT was achieved by culturing cells in adherent (gelatin) or non-adherent (PEGDA) micro-scaffold resulting in 3D stretched (ST-3D) and 3D spheroid (SP-3D) culture of HepaRG. EMT regulation is proposed as a vital consideration in designing 3D hepatic related culture configurations to promote hepatic functions for more biomimetic drug hepatotoxicity and metabolism evaluation *in vitro*.

Uniform HepaRG distribution and morphology in these two 3D *in vitro* culture configurations was validated by multiple methods. The bile canaliculus and tight junctions formed in SP-3D indicated a biomimetic micro-tissue structure. Compared with hanging drop, bioreactors and other spheroid forming methods, biomaterial assisted spheroid formation has advantages in convenience and controllability in experiments. The self-assembled tiny spheroids (diameter: 50–80 μm) also offer certain advantages for long term 3D culture without necrosis core as well as the ease for harvesting for further study or application. Drug diffusion from bulk medium to the internal cells in spheroids would be less hindered and hence improve homogeneity during drug safety evaluation.

Enhanced hepatic functions in SP-3D was validated at both gene and protein levels. To our knowledge, it represents the first systematic comparison of hepatic functions between two different 3D culture configurations with varied hepatocyte morphology. Hepatic

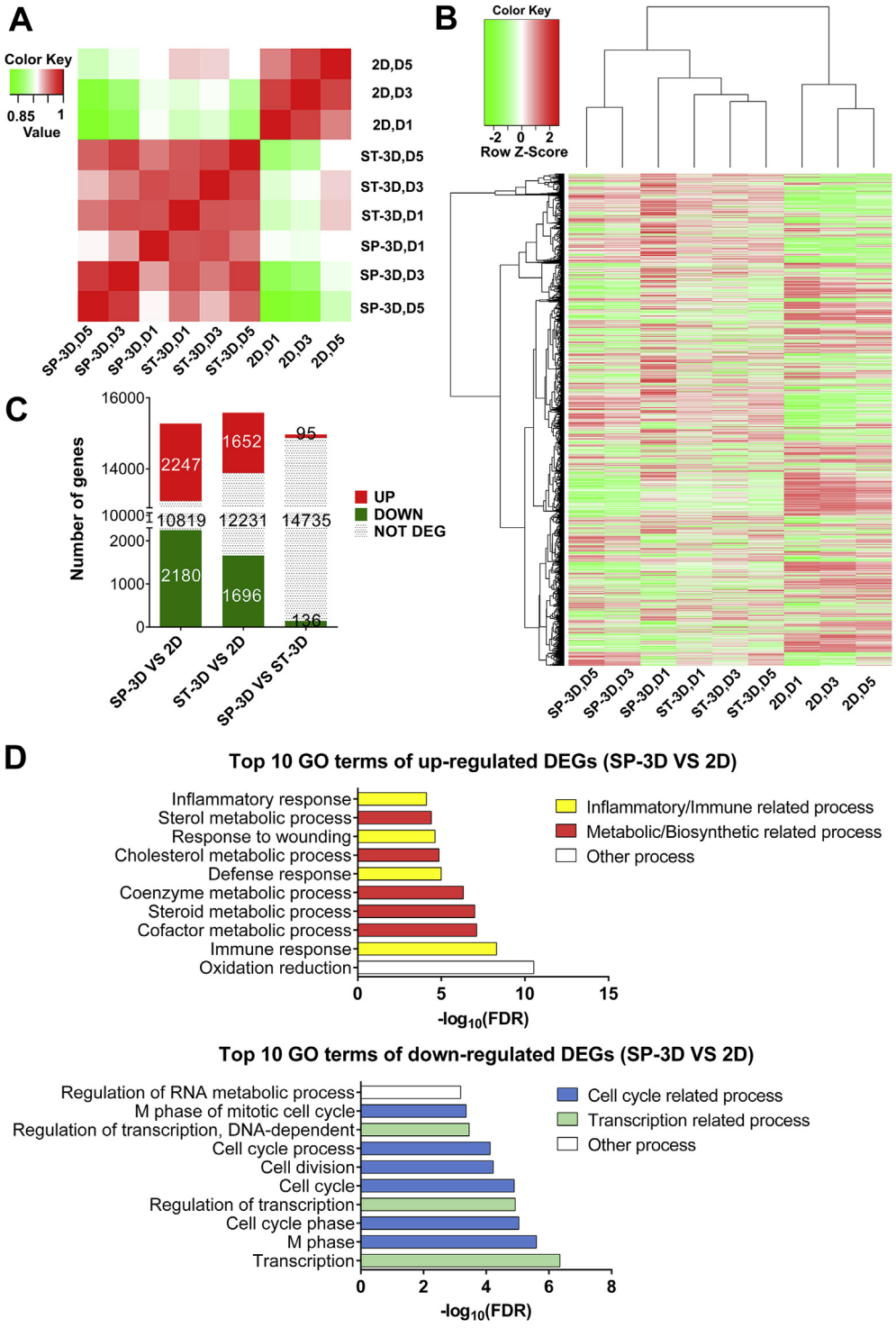

Fig. 3. Transcriptome analysis of HepaRG in 2D, ST-3D and SP-3D at Day 1, 3 and 5. A. Correlation heatmap of gene expression level in the three culture configurations. B. Bi-clustering heatmap of genes with FPKM >1 among different conditions. Samples are linked by the dendrogram above to show the similarity of their gene expression patterns. C. Number of EdgeR identified DEGs between each two culture configurations. D. Top 10 GO terms of up-regulated (top) and down-regulated (bottom) DEGs between SP-3D and 2D (Please see Table S2 for details). FDR: false discovery rate.

specific genes (*i.e. ALB, TAT, HNF4a*), nuclear receptors (*i.e. PPARα, PXR*), CYP 450s in Phase I metabolism (*i.e. CYP1A2, CYP3A4, CYP3A7*), enzymes in Phase II metabolism (*i.e. GSTA, GLUT1A1, GLUT1A3*), and transporters (*i.e. ABCC2, ABCC3* and *ABCC6*) were highly expressed in SP-3D compared with ST-3D with only one exception, *ABCB1*. As one of the most important transporters in drug resistance of hepatocytes, downregulation of *ABCB1* in SP-3D is consistent with the phenomenon in liver maturation *in vivo* and hepatic differentiation *in vitro* [9,55]. Function of MDR1 (coded by *ABCB1*) was not only relied on its expression, but also on its polarized distributions on cell membrane. After distributed on apical membrane of HepaRG, MDR1 could fulfill its function to pump out Dox even at a relatively low expression level.

E-cad accumulation was a critical feature of spheroid formation

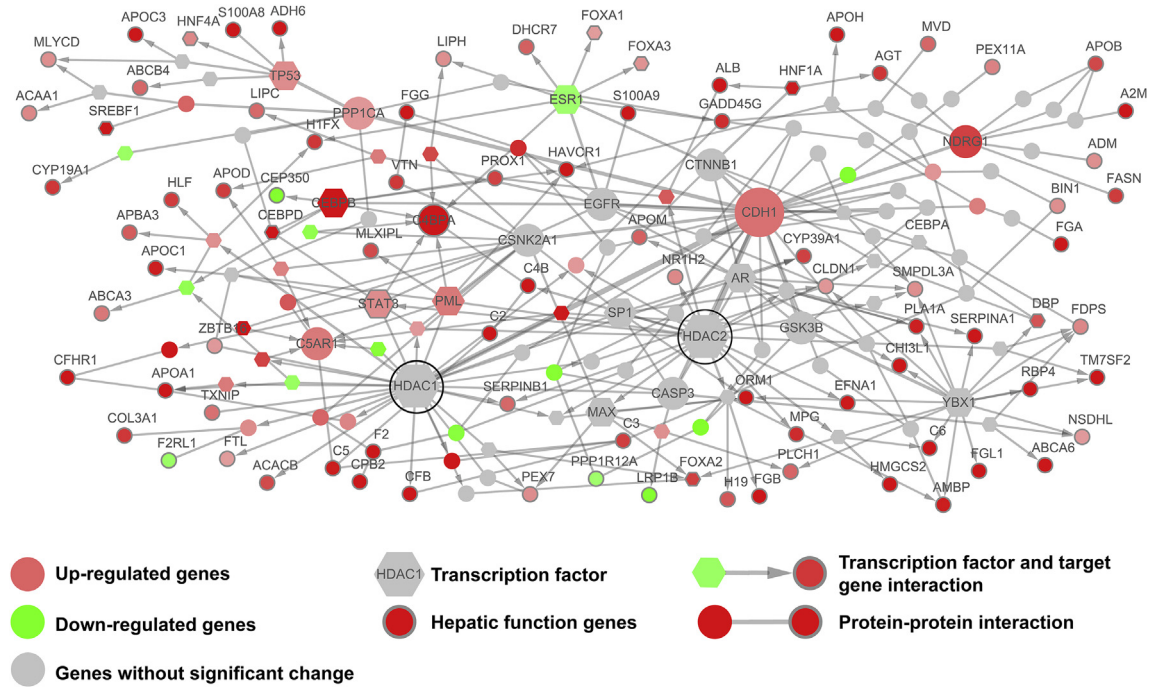

Fig. 4. Network constructed using DEGs between SP-3D and 2D as reference genes revealed HDACs as key regulators between EMT and hepatic functions. Size of each node represents the linkage betweenness of the node (Please see Table S4 for details).

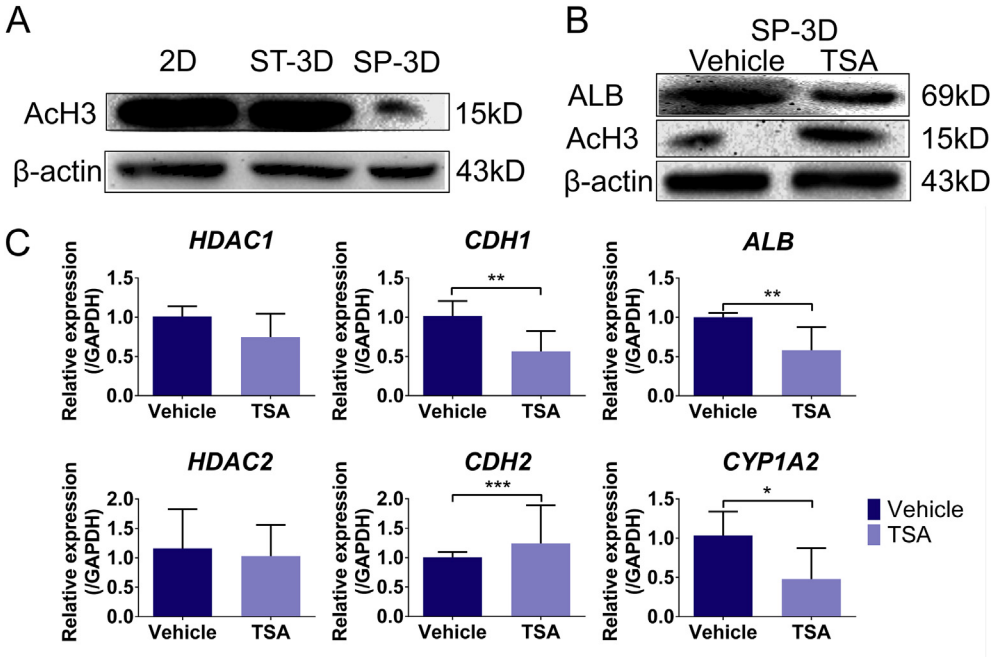

Fig. 5. Correlation of HDACs with E-cad and hepatic functions. A. WB of acetylation of histone 3 (AcH3) of HepaRG in 2D/ST-3DSP-3D. B. WB of ALB and AcH3 in SP-3D with and without treatment of HDACs inhibitor TSA. C. RT-PCR analysis of *GAPDH* normalized expression of HDACs, EMT markers and hepatic genes in SP-3D with or without TSA. (*: $P < 0.05$, **: $P < 0.01$).

according to the dynamic model proposed by Ruei-Zeng Lin et al. [56], which coincided with our observations. In suspension culture or non-adherent micro-scaffold, cells clustered through self-secreted ECM proteins and E-cad accumulated at cell-cell junctions, leading to formation of compact spheroids. Meanwhile, typical hepatocyte features such as tight junctions and micro bile canaliculus also appeared, representing a biomimetic inner structure of micro-scale hepatic spheroids. On the other hand, E-cad was the suppressor of EMT transcription factors (EMT-TF), such as Snail, Twist, N-cad, and Vimentin, so its accumulation contributed to the promotion of MET and was set as a significant signatures of MET as reported [57,58]. In our research, high expression level of *CDH1* (gene symbol of E-cad) indicated a more epithelial status of HepaRG when cultured in SP-3D than in ST-3D or 2D. Expression of

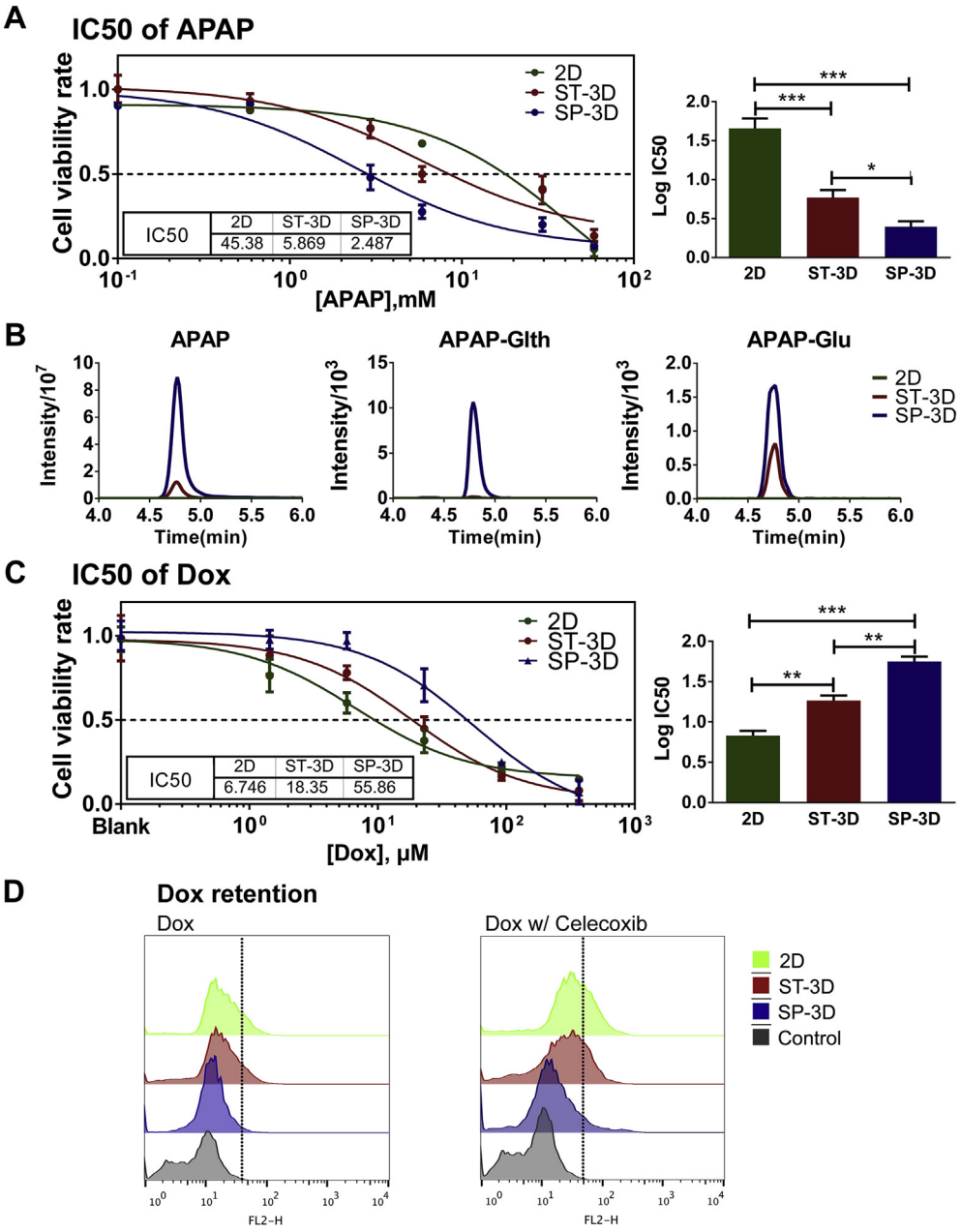

Fig. 6. Application of SP-3D and ST-3D as hepatocyte 3D culture configurations in drug toxicity and metabolism evaluation. A. Fit curve of cell viability rate of HepaRG treated with gradient APAP (left). The values of IC50 were listed in the inserted table. T test revealed significant differences of LogIC50 between each two culture configurations (right). B. LC/MS-LC analysis of APAP and its metabolite APAP-Glu/APAP-Glth. C. Fit curve of cell viability rate of HepaRG treated with gradient Dox (left). The values of IC50 were listed in the inserted table. T test revealed significant differences of LogIC50 between each two culture configurations (right). D. Flow cytometry detected Dox retention within HepaRG (left). Dox retention within HepaRG treated with Celecoxib (right). HepaRG without Dox treatment was set as negative control and the gate of fluorescence detection was indicated by the black broken line.

another epithelial marker, *EpCAM*, was consistent with the expression of *CDH1*. For mesenchymal markers, *Snail*, *Vimentin*, *Twist* and *CDH2* expression were suppressed, in SP-3D, but not in ST-3D or 2D. Such a status was quite critical for hepatocytes which belong to a typical epithelial cell type in physiological conditions. Therefore, we concluded that MET of HepaRG occurred in SP-3D. In ST-3D, apparent discrepancy of both up-regulation of epithelial and mesenchymal marker was observed from Day 3 to Day 5 (Fig. 2C–F). To explain this phenomenon, long term expression of epithelial (*CDH1*) and mesenchymal (*CDH2, Vimentin, Snail and Twist*) markers of HepaRG in 3T-3D were characterized from Day1 to Day 9 (Fig. S8). At early stage (*i.e.* from Day 1 to Day 5) of cell proliferation, all five markers exhibited the same trend as the previous data. In contrast, MET became dominant over EMT at later stage (*i.e.* from Day 5 to Day 9), where *CDH1* kept increasing while *Vimentin* and *CDH2* gradually decreased and *Snail* and *Twist* kept steady after Day 5. We hypothesized that the coincident up-regulation EMT and MET markers in ST-3D from Day 3 to Day 5 is just a temporary phenomenon in the early-stage of cell proliferation in the 3D scaffolds. At this early-stage, *CDH1* expression was enhanced with increased cell-cell interactions due to cell number growth while the proliferating HepaRG cells were still in low density in the 3D porous ST scaffold with plenty of space for cell spreading leading to sustained or even enhanced expression of

mesenchymal markers. However, MET would ultimately become dominant at later stage of cell growth in ST-3D when cell density reached confluent. It suggested that more complicated regulation of EMT/MET might exist in 3D cellular microenvironments which may be different from in normal 2D culture. Overall, EMT/MET process could be engineered using adherent/non-adherent 3D scaffolds.

To explore if there was any causal linkage between MET and promoted hepatic functions, we performed time-series analyses of gene expression profiles of markers for hepatic functions and EMT of HepaRG cultured in 2D with DMSO induction in parallel to check whether onset of MET proceed hepatic differentiation (Fig. S5). Expression of hepatic function markers (*i.e. CYP3A4*, *UGT1A1* and *ABCC2)* gradually increased during the entire culture, with the greatest jump after DMSO induction. Meanwhile, epithelial marker *(i.e. CDH1*) was up-regulated, while mesenchymal markers *(i.e. CDH2*, *Vimentin* and *Snail)* were down-regulated, and *Twist* kept steady after reaching confluence. Dramatic expression changes of hepatic functions and MET markers were both initiated after reaching confluence, which made it hard to distinguish if onset of MET preceded the up-regulation of differentiation. These data reconfirmed our previous claim in Fig. 2 regarding the concordance of MET with improved hepatic functions of HepaRG. We assume there exist complicated networks in regulation of EMT/MET and hepatic functions, and it would be difficult to directly decouple these two and clarify their causal linkage. For further investigations, large scale genomic and proteomic analysis of HepaRG cells with distinguishable EMT and differentiated status are required to reveal more detailed connections between EMT/MET and hepatic functions.

In this study, transcriptome analysis revealed *HDACs* could be critical linkage between EMT and hepatic functions. It was reported that HDAC inhibitor facilitated primary hepatocyte survival and function in 2D culture, but its function was debatable for hepatoma cell lines [59]. In hepatoma cell culture, both promotion and suppression of hepatic functions by HDAC inhibitors have been reported in the literature [23,60]. EMT and MET were both found to occur with HDAC inhibition in *in vitro* culture as well [57,61]. The inconsistency in effects of HDAC inhibition on hepatic functions and EMT may be due to that HDACs are involved in regulation of the whole genome, but not a specific signaling pathway. In our study, HDACs-mediated promotion of hepatic functions in 3D culture might be resulted from restricted gene expression by deacetylation of histones. However, the exact genes restricted by HDACs remain unknown, which needs further identification. Besides *HDACS*, transcription regulators [*e.g. tumor protein P53* (*TP53*), *Y box binding protein 1 (YBX1)* and *signal transducer and activator of transcription 3* (*STAT3*, acute-phase response factor) were also ranked with high linkage betweenness scores as revealed by transcriptome analysis, indicating potential contribution in regulation of EMT and hepatic specific genes expression. Thus, future mechanistic study will focus on histone modification or epigenetic signatures of specific hepatic genes or transcription regulators in SP-3D compared with ST-3D and 2D.

When applied in drug evaluation, HepaRG in SP-3D model shows two major advantages as compared with 2D-DMSO model. Firstly, SP-3D model is more efficient in hepatic induction than 2D-DMSO model. Hepatic functions of HepaRG in SP-3D for 5 days were comparable with that in 2D-DMSO for 28 days as represented by relatively higher ALB production (by 2 folds) and lower urea production (by 3 folds) (Fig. S7) [62]. Secondly, SP-3D model is more stable and reproducible than the 2D-DMSO counterpart. DMSO could lead to unstable cellular differentiation from batch to batch and potentially exert unpredictable and undesired influence on cell status (*e.g.* cytotoxicity). Avoid of DMSO as chemical inducer, HepaRG cultured in SP-3D model formed well-controllable spheroids (Fig. S2) with improved stability and reproducibility [63]. In this research, APAP and Dox, two well-studied drugs were utilized to test SP-3D performance in drug toxicity and metabolism evaluation. APAP is a well-known pain reliever and fever reducer with dose dependent hepatotoxicity [64,65]. Over 90% of APAP in liver is conjugated with glucuronic acid and sulfuric acid by phase II enzymes. Only a small percentage of APAP is oxidized by phase I enzyme, CYP 450s, mainly CYP 2E1, 3A4, and 1A2 to a toxic metabolite, N-acetyl-*p*-benzo-quinone imine (NAPQI). Thus, HepaRG with higher CYP 450s activity would convert more APAP to the toxic NAPQI. Hence HepaRG in SP-3D, with its lower IC50 than those of ST-3D or 2D, possess higher CYP 450s functions. Higher APAP metabolite content in HepaRG in SP-3D also revealed higher phase II enzyme activity than those in ST-3D or 2D. Dox, a commercialized anti-cancer compound in chemotherapy with cytotoxicity, on the other hand, was pumped out of hepatocytes by transporter MDR1 (about 50%) without transformation to reduce its toxicity effect [21,55]. HepaRG in SP-3D was found to be more resistance to Dox than HepaRG in ST-3D or 2D, by comparison of IC50 and Dox retention by flow cytometry, indicating better MDR1 transporter activity to enhance the efflux of Dox in hepatocyte to bile duct [47,62]. All the above evidences suggest that improved hepatic functions is in concordance with the enhanced epithelial status of hepatic cells. Hence EMT status of hepatocytes during *in vitro* culture should be taken into consideration during design of engineered 3D configurations *e.g.* scaffolds and bioreactors as well as 2D substrate with varied stiffness and topography [17,66].

In conclusion, we achieved biomaterial-engineered EMT by utilizing gelatin and PEGDA micro-scaffold which resulted in adherent ST-3D and non-adherent SP-3D culture of HepaRG respectively. Improved expressions of representative hepatic functional markers, epithelial markers, and depression of mesenchymal markers were achieved in SP-3D culture compared with ST-3D and traditional 2D culture. Transcriptome analysis and inhibition assay revealed that HDACs may be key mediating factors in regulating EMT and hepatic functions. With more bio-mimetic toxicity response, PEGDA micro-scaffold-based SP-3D culture provides an optimal culture configuration for hepatocyte-based drug toxicity evaluation. These findings indicate that precise regulation of EMT should be a vital criterion for consideration in designing hepatocyte culture configuration for basic research and application.

Disclosure of potential conflicts of interest

The authors declare that there are no conflicts of interest.

Acknowledgments

We greatly thank Prof. Sen Song from Tsinghua University and Tao Yu for the help in construction of plasmid containing ALB promoter-EGFP sequence. We are grateful to Xiaohui Liu and Xueying Wang for the help in LC/MS-LC detection. We thank Qinghai Dai and Bokai Song for the help in imaging experiments and all Du-lab members for general help. This work is financially supported by Natural Science Foundation of China (Grant No: 51273106, 81201474, 91019016, 31361163004, 31301044), National Basic Research Program of China (Grant No: 2012CB316503) and Beijing Municipal Natural Science Foundation (Grant No: 157142090).

Appendix A. Supplementary data

Supplementary data related to this article can be found at http://dx.doi.org/10.1016/j.biomaterials.2016.03.001.

References

[1] S.M. Paul, et al., How to improve R&D productivity: the pharmaceutical industry's grand challenge, Nat. Rev. Drug Discov. 9 (3) (2010) 203–214.
[2] N.J. Hewitt, et al., Primary hepatocytes: current understanding of the regulation of metabolic enzymes and transporter proteins, and pharmaceutical practice for the use of hepatocytes in metabolism, enzyme induction, transporter, clearance, and hepatotoxicity studies, Drug Metab. Rev. 39 (1) (2007) 159–234.
[3] K. Takayama, et al., Efficient generation of functional hepatocytes from human embryonic stem cells and induced pluripotent stem cells by HNF4alpha transduction, Mol. Ther. 20 (1) (2012) 127–137.
[4] A. Guillouzo, et al., The human hepatoma HepaRG cells: a highly differentiated model for studies of liver metabolism and toxicity of xenobiotics, Chem. Biol. Interact. 168 (1) (2007) 66–73.
[5] Z. Xu, J. Wang, Y. Du, Recent advances in embryonic stem cell engineering toward tailored lineage differentiation, in: M.K. Danquah, R.I. Mahato (Eds.), Emerging Trends in Cell and Gene Therapy, Humana Press, 2013, pp. 33–54.
[6] P. Gunness, et al., 3D organotypic cultures of human HepaRG cells: a tool for in vitro toxicity studies, Toxicol. Sci. 133 (1) (2013) 67–78.
[7] T.T. Chang, M. Hughes-Fulford, Monolayer and spheroid culture of human liver hepatocellular carcinoma cell line cells demonstrate distinct global gene expression patterns and functional phenotypes, Tissue Eng. Part A 15 (3) (2009) 559–567.
[8] M. Kawada, et al., Massive culture of human liver cancer cells in a newly developed radial flow bioreactor system: ultrafine structure of functionally enhanced hepatocarcinoma cell lines, In Vitro Cell Dev. Biol. Anim. 34 (2) (1998) 109–115.
[9] T. Elkayam, et al., Enhancing the drug metabolism activities of C3A – a human hepatocyte cell line–by tissue engineering within alginate scaffolds, Tissue Eng. 12 (5) (2006) 1357–1368.
[10] A. Treyer, A. Musch, Hepatocyte polarity, Compr. Physiol. 3 (1) (2013) 243–287.
[11] C.M. Nelson, et al., Change in cell shape is required for matrix metalloproteinase-induced epithelial-mesenchymal transition of mammary epithelial cells, J. Cell. Biochem. 105 (1) (2008) 25–33.
[12] G. Moreno-Bueno, F. Portillo, A. Cano, Transcriptional regulation of cell polarity in EMT and cancer, Oncogene 27 (55) (2008) 6958–6969.
[13] M.A. Nieto, Epithelial plasticity: a common theme in embryonic and cancer cells, Science 342 (6159) (2013) 1234850.
[14] D.L. Franco, et al., Snail1 suppresses TGF-beta-induced apoptosis and is sufficient to trigger EMT in hepatocytes, J. Cell Sci. 123 (Pt 20) (2010) 3467–3477.
[15] D. Schneider, M. Tarantola, A. Janshoff, Dynamics of TGF-beta induced epithelial-to-mesenchymal transition monitored by electric cell-substrate impedance sensing, Biochim. Biophys. Acta 1813 (12) (2011) 2099–2107.
[16] C.M. Nelson, et al., Change in cell shape is required for matrix metalloproteinase-induced epithelial-mesenchymal transition of mammary epithelial cells, J. Cell Biochem. 105 (1) (2008) 25–33.
[17] J.W. O'Connor, E.W. Gomez, Cell adhesion and shape regulate TGF-beta1-induced epithelial-myofibroblast transition via MRTF-A signaling, PLoS One 8 (12) (2013) e83188.
[18] T.L. Downing, et al., Biophysical regulation of epigenetic state and cell reprogramming, Nat. Mater 12 (12) (2013) 1154–1162.
[19] S.C. Wei, et al., Matrix stiffness drives epithelial-mesenchymal transition and tumour metastasis through a TWIST1-G3BP2 mechanotransduction pathway, Nat. Cell Biol. 17 (5) (2015) 678–688.
[20] W. Liu, et al., Magnetically controllable 3D microtissues based on magnetic microcryogels, Lab. Chip 14 (15) (2014) 2614–2625.
[21] X. Li, et al., Micro-scaffold array chip for upgrading cell-based high-throughput drug testing to 3D using benchtop equipment, Lab. Chip 14 (3) (2014) 471–481.
[22] S. Zhao, et al., Glycerol-mediated nanostructure modification leading to improved transparency of porous polymeric scaffolds for high performance 3D cell imaging, Biomacromolecules 15 (7) (2014) 2521–2531.
[23] A.J. de Ruijter, et al., Histone deacetylases (HDACs): characterization of the classical HDAC family, Biochem. J. 370 (Pt 3) (2003) 737–749.
[24] C.C. DuFort, M.J. Paszek, V.M. Weaver, Balancing forces: architectural control of mechanotransduction, Nat. Rev. Mol. Cell Biol. 12 (5) (2011) 308–319.
[25] N.M. Ramdas, G.V. Shivashankar, Cytoskeletal control of nuclear morphology and chromatin organization, J. Mol. Biol. 427 (3) (2015) 695–706.
[26] N. Jain, et al., Cell geometric constraints induce modular gene-expression patterns via redistribution of HDAC3 regulated by actomyosin contractility, Proc. Natl. Acad. Sci. U. S. A. 110 (28) (2013) 11349–11354.
[27] A. Moreau, et al., Xenoreceptors CAR and PXR activation and consequences on lipid metabolism, glucose homeostasis, and inflammatory response, Mol. Pharm. 5 (1) (2008) 35–41.
[28] R. Hoekstra, et al., Phase 1 and phase 2 drug metabolism and bile acid production of HepaRG cells in a bioartificial liver in absence of dimethyl sulfoxide, Drug Metab. Dispos. 41 (3) (2013) 562–567.
[29] T.B. Andersson, K.P. Kanebratt, J.G. Kenna, The HepaRG cell line: a unique in vitro tool for understanding drug metabolism and toxicology in human, Expert Opin. Drug Metab. Toxicol. 8 (7) (2012) 909–920.
[30] H.H. Gerets, et al., Characterization of primary human hepatocytes, HepG2 cells, and HepaRG cells at the mRNA level and CYP activity in response to inducers and their predictivity for the detection of human hepatotoxins, Cell Biol. Toxicol. 28 (2) (2012) 69–87.
[31] C. Aninat, et al., Expression of cytochromes P450, conjugating enzymes and nuclear receptors in human hepatoma HepaRG cells, Drug Metab. Dispos. 34 (1) (2006) 75–83.
[32] M. Lubberstedt, et al., HepaRG human hepatic cell line utility as a surrogate for primary human hepatocytes in drug metabolism assessment in vitro, J. Pharmacol. Toxicol. Methods 63 (1) (2011) 59–68.
[33] P. Gripon, et al., Infection of a human hepatoma cell line by hepatitis B virus, Proc. Natl. Acad. Sci. U. S. A. 99 (24) (2002) 15655–15660.
[34] A. Xiong, et al., Isolation of human fetal liver progenitors and their enhanced proliferation by three-dimensional coculture with endothelial cells, Tissue Eng. Part A 14 (6) (2008) 995–1006;
[35] A comment on 'global activity of cancer registries and cancer control and cancer incidence statistics in Korea', J. Prev. Med. Public Health 41 (3) (2008) 208–209 (Author reply 209-11).
[36] Y. Li, et al., Primed 3D injectable microniches enabling low-dosage cell therapy for critical limb ischemia, Proc. Natl. Acad. Sci. U. S. A. 111 (37) (2014) 13511–13516.
[37] R. Yao, et al., Hepatic differentiation of human embryonic stem cells as microscaled multilayered colonies leading to enhanced homogeneity and maturation, Small 10 (21) (2014) 4311–4323.
[38] X. Yan, et al., A ready-to-use, versatile, multiplex-able three-dimensional scaffold-based immunoassay chip for high throughput hepatotoxicity evaluation, Lab. Chip 15 (12) (2015) 2634–2646.
[39] C. Trapnell, et al., Differential gene and transcript expression analysis of RNA-seq experiments with TopHat and Cufflinks, Nat. Protocol 7 (3) (2012) 562–578.
[40] M.D. Robinson, D.J. McCarthy, G.K. Smyth, edgeR: a bioconductor package for differential expression analysis of digital gene expression data, Bioinformatics 26 (1) (2010) 139–140.
[41] W. Huang da, B.T. Sherman, R.A. Lempicki, Systematic and integrative analysis of large gene lists using DAVID bioinformatics resources, Nat. Protocol 4 (1) (2009) 44–57.
[42] G. Csardi, T. Nepusz, The igraph software package for complex network research, Int. J. Complex Syst. 1695 (5) (2006) 1–9.
[43] T.S. Keshava Prasad, et al., Human protein reference database – 2009 update, Nucl. Acids Res. 37 (2009) D767–D772 (Database issue).
[44] L.A. Bovolenta, M.L. Acencio, N. Lemke, HTRIdb: an open-access database for experimentally verified human transcriptional regulation interactions, BMC Genomics 13 (2012) 405.
[45] P.L. Flom, et al., A new measure of linkage between two sub-networks, Connections 26 (1) (2004) 62–70.
[46] J. Taunton, C.A. Hassig, S.L. Schreiber, A mammalian histone deacetylase related to the yeast transcriptional regulator Rpd3p, Science 272 (5260) (1996) 408–411.
[47] H.J. Alter, B.S. Blumberg, Further studies on a "new" human isoprecipitin system (Australia antigen), Blood 27 (3) (1966) 297–309.
[48] Satish G. Pingale, K.V. M, Quantification of lumefantrine in human plasma using LC-MS/MS and its application to a bioequivalence study, J. Pharm. 2013 (2013) 8 (Article ID 437697).
[49] W. Liu, et al., Microcryogels as injectable 3-D cellular microniches for site-directed and augmented cell delivery, Acta Biomater. 10 (5) (2014) 1864–1875.
[50] O. Fardel, et al., Overexpression of the multidrug resistance gene product in adult rat hepatocytes during primary culture, Eur. J. Biochem. 205 (2) (1992) 847–852.
[51] P. Godoy, et al., Extracellular matrix modulates sensitivity of hepatocytes to fibroblastoid dedifferentiation and transforming growth factor beta-induced apoptosis, Hepatology 49 (6) (2009) 2031–2043.
[52] S. Ng, et al., Improved hepatocyte excretory function by immediate presentation of polarity cues, Tissue Eng. 12 (8) (2006) 2181–2191.
[53] Z. Liu, et al., RUNX3 regulates vimentin expression via miR-30a during epithelial-mesenchymal transition in gastric cancer cells, J. Cell Mol. Med. 18 (4) (2014) 610–623.
[54] H. Peinado, D. Olmeda, A. Cano, Snail, Zeb and bHLH factors in tumour progression: an alliance against the epithelial phenotype? Nat. Rev. Cancer 7 (6) (2007) 415–428.
[55] K.R. Roy, et al., Celecoxib inhibits MDR1 expression through COX-2-dependent mechanism in human hepatocellular carcinoma (HepG2) cell line, Cancer Chemother. Pharmacol. 65 (5) (2010) 903–911.
[56] R.Z. Lin, et al., Dynamic analysis of hepatoma spheroid formation: roles of E-cadherin and beta1-integrin, Cell Tissue Res. 324 (3) (2006) 411–422.
[57] H. Peinado, et al., Snail mediates E-cadherin repression by the recruitment of the Sin3A/histone deacetylase 1 (HDAC1)/HDAC2 complex, Mol. Cell Biol. 24 (1) (2004) 306–319.
[58] K. Vuoriluoto, et al., Vimentin regulates EMT induction by Slug and oncogenic H-Ras and migration by governing Axl expression in breast cancer, Oncogene 30 (12) (2011) 1436–1448.
[59] G. Elaut, et al., A metabolic screening study of trichostatin A (TSA) and TSA-like histone deacetylase inhibitors in rat and human primary hepatocyte cultures, J. Pharmacol. Exp. Ther. 321 (1) (2007) 400–408.
[60] N.E. Aguilar-Olivos, et al., The role of epigenetics in the progression of non-alcoholic fatty liver disease, Mini Rev. Med. Chem. 15 (14) (2015) 1187–1194.
[61] A. Kaimori, et al., Histone deacetylase inhibition suppresses the transforming

growth factor beta1-induced epithelial-to-mesenchymal transition in hepatocytes, Hepatology 52 (3) (2010) 1033–1045.
[62] S.P. Rebelo, et al., HepaRG microencapsulated spheroids in DMSO-free culture: novel culturing approaches for enhanced xenobiotic and biosynthetic metabolism, Arch. Toxicol. 89 (8) (2015) 1347–1358.
[63] A. Schulze, et al., Hepatocyte polarization is essential for the productive entry of the hepatitis B virus, Hepatology 55 (2) (2012) 373–383.
[64] S. Tobwala, et al., Comparative evaluation of N-acetylcysteine and N-acetylcysteineamide in acetaminophen-induced hepatotoxicity in human hepatoma HepaRG cells, Exp. Biol. Med. (Maywood) 240 (2) (2015) 261–272.
[65] S.B. Leite, et al., Three-dimensional HepaRG model as an attractive tool for toxicity testing, Toxicol. Sci. 130 (1) (2012) 106–116.
[66] T.T. Chang, M. Hughes-Fulford, Molecular mechanisms underlying the enhanced functions of three-dimensional hepatocyte aggregates, Biomaterials 35 (7) (2014) 2162–2171.